Inorganic Chemistry

Article

pubs.acs.org/IC

Detection of the Singlet and Triplet MM $\delta\delta^*$ States in Quadruply Bonded Dimetal Tetracarboxylates (M = Mo, W) by Time-Resolved Infrared Spectroscopy

Brian G. Alberding, Malcolm H. Chisholm,* and Terry L. Gustafson*

Department of Chemistry, The Ohio State University, 100 West 18th Avemue, Columbus, Ohio 43210-1185, United States

Supporting Information

ABSTRACT: The compounds $M_2(O_2C^tBu)_4$ and $M_2(O_2CC_6H_5)_4$, where M = Mo or W, have been examined by femtosecond time-resolved IR (fs-TRIR) spectroscopy in tetrahydrofuran with excitation into the singlet metal-to-ligand charge-transfer (^{1}MLCT) band. In the region from 1500 to 1600 cm^{-1}, a long-lived excited state (>2 ns) has been detected for the compounds $M_2(O_2C^tBu)_4$ and $Mo_2(O_2C-C_6H_5)_4$ with an IR absorption at ~1540 cm^{-1} assignable to the asymmetric CO_2 stretch, $\nu_{as}(CO_2)$, of the triplet metal−metal $\delta-\delta$ star (^{3}MM $\delta\delta^*$) state. The fs-TRIR spectra of $W_2(O_2C-C_6H_5)_4$ are notably different and are assigned to decay of the MLCT states. In ^{3}MM $\delta\delta^*$, the removal of an electron from the δ orbital reduces MM δ to CO_2 π^* back-bonding and causes a shift of $\nu_{as}(CO_2)$ to higher energy by ~30−60 cm^{-1}, depending on the metal. TRIR spectroscopy also provides evidence for $M_2(O_2C^tBu)_4$, where M = Mo or W, having MM $\delta\delta^*$ S_1 states with $\nu_{as}(CO_2)$ distinct from those of the ^{3}MM $\delta\delta^*$ states.

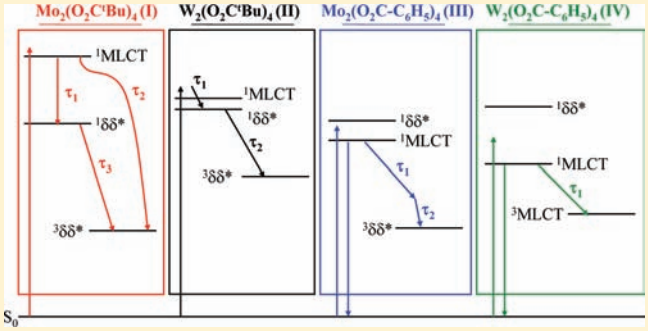

INTRODUCTION

Metal−metal (MM) quadruply bonded complexes share the common ground-state electronic configuration MM $\sigma^2\pi^4\delta^2$, and photoexcitation can lead to promotion of an electron from the δ orbital to the δ^* orbital. The observation of the $^1\delta\delta^*$ transition has been of considerable interest over the years with some initial concern about the interpretation of the energy of the transition with regard to the strength of the δ bond.[1] The initial concern arose from the observation that the single-electron promotion $^2\delta\delta^*$ in compounds with ground-state configuration MM $\sigma^2\pi^4\delta^1$ was at much lower energy. Nocera noted, "Two electrons in weakly coupled orbitals on two centers give rise to four states: two low-energy diradical states arising from one electron in each orbital with spins opposed (singlet) and parallel (triplet), respectively, and two higher energy zwitterionic singlet states derived from the anti-symmetric and symmetric linear combinations, respectively, in which both electrons are paired in one orbital of either center."[2] Of this manifold of states, the two at highest energy were detected by two-photon spectroscopy. Subsequently, Cotton and Nocera noted that studies of the MM δ orbital had led to "The Whole Story of the Two-Electron Bond, with the δ Orbital as a Paradigm."[3]

We reasoned that detection of the $\delta\delta^*$ states should be possible by ultrafast time-resolved vibrational spectroscopy. In principle, time-resolved Raman spectroscopy should reveal a significant shift in the magnitude of ν(MM) because in the ground state there is a bond of order 4, and in the excited $\delta\delta^*$ state, the bond order is only 3. While ground-state resonance Raman spectroscopy affords the ease of observation of ν(MM) along with its overtones and combination bands in many complexes,[4,5] the requirement for the observation of resonance enhancement in the excited state depends upon the presence of intense excited-state absorption.[6,7] This matter of femtosecond to nanosecond triplet time-resolved studies is of continuing interest in this group. We report here, however, that the ^{3}MM $\delta\delta^*$ state can readily be detected by femtosecond time-resolved IR (fs-TRIR) spectroscopy in certain dimetal carboxylates by the shift in $\nu_{as}(CO_2)$.

From earlier photophysical studies on $M_2(O_2CR)_4$ complexes where M = Mo or W, we have been able to detect both singlet and triplet excited states for certain MM quadruply bonded compounds having carboxylate ligands. The singlets have been assigned as ^{1}MLCT (where MLCT = metal-to-ligand charge transfer) and the triplets as either ^{3}MLCT or ^{3}MM $\delta\delta^*$.[8−10] Evidence for the latter came from the lack of solvent dependence and the appearance of vibronic features with ν(MM) ~ 400 cm^{-1} in the emission from this state. In general, when M = Mo, photophysical deactivation involves the ^{1}MLCT to ^{3}MM $\delta\delta^*$ pathway unless the ligands have extremely low-lying π^* orbitals and T_1 becomes ^{3}MLCT. Conversely, when M = W, photophysical deactivation involves the ^{1}MLCT to ^{3}MLCT pathway unless the ligand π^* orbitals lie at extremely high energy and T_1 is ^{3}MM $\delta\delta^*$. In this case, only one example

Received: September 6, 2011
Published: November 30, 2011

   dx.doi.org/10.1021/ic201957a | Inorg. Chem. 2012, 51, 491−498

has been found where a $W_2(O_2CR)_4$ complex has T_1 as ^{3}MM $\delta\delta^*$, and it is the complex where R = 2,4,6-triisopropylbenzene.[8]

In this work, we have hoped to push the tunability of the ligand π^* orbitals to the extreme high-energy limit by examining the complexes $M_2(O_2C^tBu)_4$, where M = Mo (**I**) or W (**II**). In this way, greater support for the WW $\delta\delta^*$ state could be obtained or more complex initial dynamics could be observed by pushing the MLCT states from S_1 to S_2. It has been difficult to find both excitation sources and detection equipment suitable when the MLCT absorptions are pushed to the extreme high energy using visible transient absorption and vis−near-IR emission, as we have done previously. Given that for carboxylate ligands the filled MM δ orbital interacts with the empty CO_2 π^* orbital of symmetry b_{2g} in the D_{4h} point group, back-bonding in the $\delta\delta^*$ state should be less than that in the ground state. It thus occurred to us that time-resolved infrared (TRIR) spectroscopy could also be a useful technique to probe the nature of the photoexcited states of molecules of the type $M_2(O_2CR)_4$ by $\nu_{as}(CO_2)$ vibrations. We also decided to study $M_2(O_2CC_6H_5)_4$, where M = Mo (**III**) or W (**IV**), for comparison, where the orbital energies are closer to the regime that we previously studied and the dynamics are expected to be more conventional toward our earlier findings.

EXPERIMENTAL SECTION

The compounds $Mo_2(O_2C^tBu)_4$ (**I**),[8] $W_2(O_2C^tBu)_4$ (**II**),[9] $Mo_2(O_2C-C_6H_5)_4$ (**III**),[8] and $W_2(O_2C-C_6H_5)_4$ (**IV**)[10] were synthesized according to literature procedures. All solutions were prepared in tetrahydrofuran (THF) and transferred to the sample cell in a glovebox using standard techniques. The THF solvent was distilled, degassed, and stored over molecular sieves prior to use.

Electronic structure calculations were carried out on simplified model compounds of the type $M_2(O_2CH)_4$ in order to show the dependence of orbital energies on the nature of the metal. The calculations were carried out using density functional theory (DFT) in the *Gaussian 03* suite of programs (revision D.01[11]) to optimize the gas-phase geometry of the model compounds in D_{4h} symmetry. The B3LYP functional was used along with the 6-31+G* basis set for carbon, hydrogen, and oxygen, while the SDD energy-consistent pseudopotential was used for molybdenum and tungsten. Optimization was confirmed to be a minimum on the potential energy surface by frequency analysis, and the orbital analysis (isosurface value = 0.02) was completed using *GaussView*.

Absorption spectra at room temperature were obtained using a Perkin-Elmer Lambda 900 spectrometer. The spectra were collected using the same sample cell as that used for the IR measurements. Molar absorptivities indicated in Figure 2 were obtained from literature sources with the exception of **III**, whose reported literature value is incorrect. The molar absorptivity of this compound was determined by dissolving ∼0.6 mg into 50 mL of THF and measuring the absorbance in a 1-cm-path-length quartz cuvette equipped with a Kontes top and sealed with a Teflon tap. The value for the reported molar absorptivity reported in Figure 2 was obtained in this way.

The laser system for the TRIR setup utilizes a Ti:sapphire oscillator and regenerative amplifier combination operating at 1 kHz that was described in detail previously.[12] The fundamental laser beam is split to pump either an SFG or UV/vis OPA to produce pump pulses tunable throughout the visible spectrum and a DFG OPA to produce mid-IR pulses (2−10 μm). Light of 400 nm is produced by frequency doubling of the fundamental 800 nm pulse. The IR beam is split into a probe and a reference beam by a Ge beamsplitter. Each is focused onto the sample cell where only the probe is overlapped with the pump beam. After the sample, the probe and reference beams are directed to a grating spectrometer (Triax 320) and spectrally dispersed onto separate Hg−Cd−Te array (32 elements) detectors cooled by liquid nitrogen. The pump and probe pulses are synchronized by passing the pump pulse through a chopper operating at 500 Hz, allowing for measurement of the probe signal under pump on/off conditions. The corresponding absorbance signal from the reference beam is subtracted to obtain the overall signal. The TRIR setup was also described previously.[13]

TRIR samples were sealed in a Perkin-Elmer rectangular semi-demountable cell with a 0.1 mm Teflon spacer between a 4-mm-thick CaF_2 back window and 2-mm-thick CaF_2 front window in a glovebox. THF was the solvent, and the concentration was such that the absorbance was ∼1.0−2.0 at the MLCT λ_{max}. During measurements, the static sample cell was periodically translated manually using an XYZ stage. Absorption spectra were obtained before and after measurements to ensure that no photodecomposition had occurred. Samples were excited into the MLCT bands for **I**−**IV** with source wavelengths of 310, 400, 400, and 514 nm, respectively.

RESULTS AND DISCUSSION

Bonding Considerations. The bonding in a typical paddlewheel molecule of the form L_4MML_4 with D_{4h} symmetry leads to the well-known MM bonding configuration $\sigma\pi\pi\delta\delta^*\pi^*\pi^*\sigma^*$ for the metal-based orbitals, and in D_{4h} symmetry, the δ and δ^* orbitals transform as b_{2g} and b_{1u}, respectively. For the MM quadruply bonded complex ions $Re_2Cl_8^{2-}$ and $Mo_2Cl_8^{4-}$, the MM configuration $\sigma^2\pi^4\delta^2$ is valid and the lowest-energy electronic transition is the singlet $\delta \rightarrow \delta^*$ transition $^1A_{1g} \rightarrow {}^1A_{2u}$. However, in dimetal tetracarboxylates having MM quadruple bonds, there are further interactions that perturb this simple bonding description. These arise from the carboxylate π-type orbitals, and in a molecule such as $Mo_2(O_2CH)_4$, which has rigorous D_{4h} symmetry, the bonding π set derived from I (shown below) transforms as a_{2g}, e_u, and b_{2g}, the CO_2 π^* set, shown in III, transforms as a_{2g}, e_u, and b_{2g},

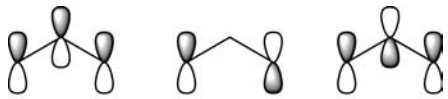

I II III

and the nonbonding p π lone pairs, II, transform as a_{1u}, e_g, and b_{1u}.

Typically, the orbital energy of the MM δ^2 orbital falls in the range of −4 to −6 eV, and thus with the large electronegativity of oxygen, the filled CO_2 orbital of b_{2g} symmetry has a relatively small interaction with the MM δ orbital. Similarly, the CO_2 nonbonding oxygen lone-pair combination of b_{1u} symmetry has a very small interaction with the MM δ^* orbital. Thus, the principal interaction based on orbital energies and overlap involves the filled MM δ orbital and the CO_2 π^* orbital of b_{2g} symmetry. For related compounds of the form $M_2(O_2CR)_4$, where M = Mo or W, the W δ orbital lies higher in energy by ∼0.5 eV, thus making this MM δ to CO_2 π^* orbital more important for M = W.[4] If the oxygen atoms of the carboxylate are replaced by S or NR groups, the higher energy of the filled ligand π orbitals derived from I and II causes them to mix more strongly with the MM δ and δ^* orbitals.

Of course with the aid of computational methods based on DFT, these qualitative considerations can be laid on a more quantitative basis, and the calculated frontier molecular orbital energy level diagram for the molecules $M_2(O_2CH)_4$ are shown in Figure 1. For both M = Mo and W, the energy diagram shown in Figure 1 leads to the expectation that the lowest-energy electronic transition will be a $^1(\delta \rightarrow \delta^*)$ transition with MM δ to CO_2 π^* at higher energy. Because of the relatively

dx.doi.org/10.1021/ic201957a | *Inorg. Chem.* 2012, 51, 491−498

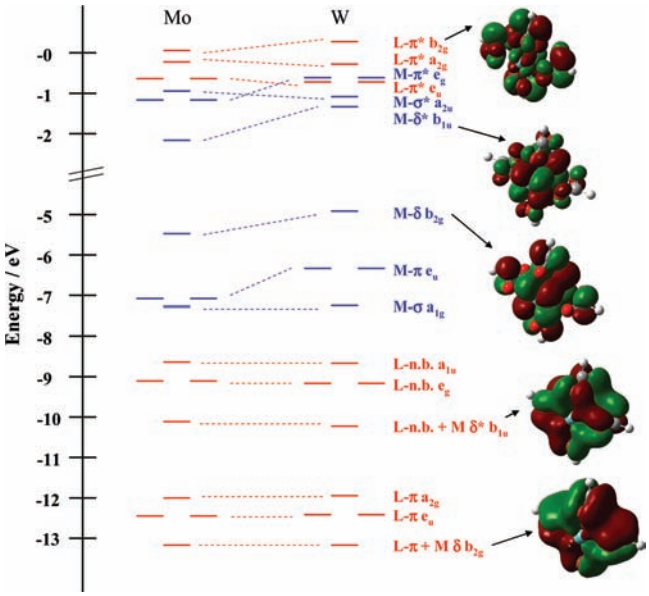

Figure 1. Frontier molecular orbital energy diagram for simplified compounds of the type $M_2(O_2CH)_4$ where M = Mo (left) or W (right). Orbitals with primarily metal contribution are shown in blue, and those with primarily of ligand contribution are shown in red.

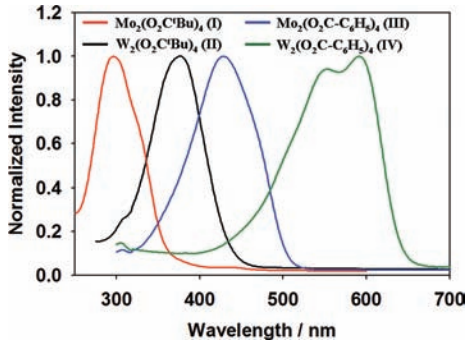

Figure 2. Absorption spectra of compounds **I** (red), **II** (black), **III** (blue), and **IV** (green). Relative intensities are indicated by the molar absorptivity measured at λ_{max}: ε(296 nm) = 10 000 M^{-1} cm^{-1} (**I**);[9] ε(378 nm) = 12 600 M^{-1} cm^{-1} (**II**);[9] ε(427 nm) = 20 000 M^{-1} cm^{-1} (**III**); ε(592 nm) = 33 100 M^{-1} cm^{-1} (**IV**).[17]

weak metal d−d overlap in the δ orbital, the oscillator strength of this transition is also relatively weak, while that of the MM δ to CO_2 π^* transition is a fully allowed MLCT and is much more intense. For this reason, $W_2(O_2CR)_4$ compounds, where R = alkyl, often do not exhibit a $^1(\delta \rightarrow \delta^*)$ transition because it is masked by the intense close-energy fully allowed ^{1}MLCT involving CO_2 π^*. If the R group in a $M_2(O_2CR)_4$ molecule contains a conjugated π system that directly interacts with the CO_2 π system, for instance, as in the benzoate ligand, then the ^{1}MLCT band is moved to even lower energy and becomes the lowest-energy fully allowed electronic transition.

The absorption spectra for the compounds $M_2(O_2C^tBu)_4$ [M = Mo (**I**) and W (**II**)] and $M_2(O_2CPh)_4$ [M = Mo (**III**) and W (**IV**)] are shown in Figure 2 and nicely verify the expectations outlined above. Notably, only for **I** is the $^1(\delta \rightarrow \delta^*)$ transition seen as a very weak absorption at $\lambda \sim 450$ nm with $\varepsilon \sim 100$ M^{-1} cm^{-1}, and as the energy of the ^{3}MLCT band decreases, its energy increases. The intense transitions are the MLCT absorptions between the M δ b_{2g} orbital and the L π^* e_u orbitals, which become lower energy by changing the metal from Mo to W and by changing the ligand from pivalate to benzoate. Consequently, in **II**−**IV**, the weak $\delta\delta^*$ transition becomes masked by the much stronger MLCT transition and is not observed. Additionally, the $\delta\delta^*$ transition is shifted to slightly higher energy by making equivalent changes. This is suggested by the calculations in Figure 1 for these complexes and has been shown experimentally by the emission spectra in related complexes.[8] Furthermore, it has also been demonstrated in related complexes that increasing the electron-withdrawing ability of the ligands can lead to a slightly higher-energy $\delta\delta^*$ transition.[17] These trends are also consistent with expectations that the intensity of a MLCT band is related to the energy separation of the two states and the overlap of the orbitals, which is reflected in the reported molar absorptivity values. One final comment concerning the absorption spectra considers the bandshapes observed. They are asymmetric, and in the case of **IV**, there are clearly two resolved bands. Studies on related compounds have shown similar features that sharpen and shift to lower energy upon cooling to 77 K. Therefore, these contributions to the absorption spectra are identified as vibronic features.[18]

fs-TRIR Spectroscopy: Long-Lived Spectra. The fs-TRIR apparatus utilized in this work can monitor processes occurring from approximately 100 fs to 3 ns. Each compound studied undergoes some initial picosecond dynamics, but a common feature is that a long-lived species remains present afterward, as shown in Figures 3−6. In compounds **I**−**III**, this long-lived species is represented by well-resolved peaks at 1549, 1540, and 1540 cm^{-1}, respectively. Because these peaks occur with similar shapes and at similar wavenumbers, this implies similar electronic environments about the carboxylate group in each species. Furthermore, although the peak frequencies are similar, the shift compared to the ground-state wavenumber is also important. For **I**−**III**, this value is 31, 28, and 60 cm^{-1} to higher wavenumber, respectively, and it should be noted that the shift is larger for tungsten because of the greater degree of back-bonding when this metal is present. Notably, the long-lived spectrum for compound **IV** is different. It was collected in a similar part of the IR spectrum, 1570−1470 cm^{-1}, but consists of a very broad band across the entire region with several apparent features and bleaching at 1490 cm^{-1}.

It is proposed that the peak near 1540 cm^{-1} occurring at long delay times is due to the $^3(\delta \rightarrow \delta^*)$ state and that in **IV** the broad spectrum results from the T_1 state being ^{3}MLCT. The shift to higher wavenumber is consistent with the $\delta\delta^*$ assignment. Calculations have shown that the highest occupied molecular orbital (HOMO) in these types of compounds contains CO_2 π^* character due to back-bonding with the M δ orbital.[4,17] Removal of an electron from this orbital to δ^* decreases the π^* character of the CO_2 bonds and reduces the degree of back-bonding, which results in the upward shift of this vibrational mode. The broad spectrum in **IV** possibly results from the reduction of ligand vibrations associated with the phenyl ring or, more likely, a very low-energy excited-state electronic transition (vide infra).

Previously, a range of techniques have been used to differentiate between the $^3(\delta \rightarrow \delta^*)$ and ^{3}MLCT states in related "trans-bis-bis" compounds.[15,16,18] In general, when the metal is Mo, the T_1 state is $^3(\delta \rightarrow \delta^*)$, and for tungsten, it is ^{3}MLCT. Only when the L π^* orbital is very low in energy is the assignment for molybdenum reversed and, conversely, only when the L π^* orbital is very high in energy is that true for

dx.doi.org/10.1021/ic201957a | Inorg. Chem. 2012, 51, 491−498

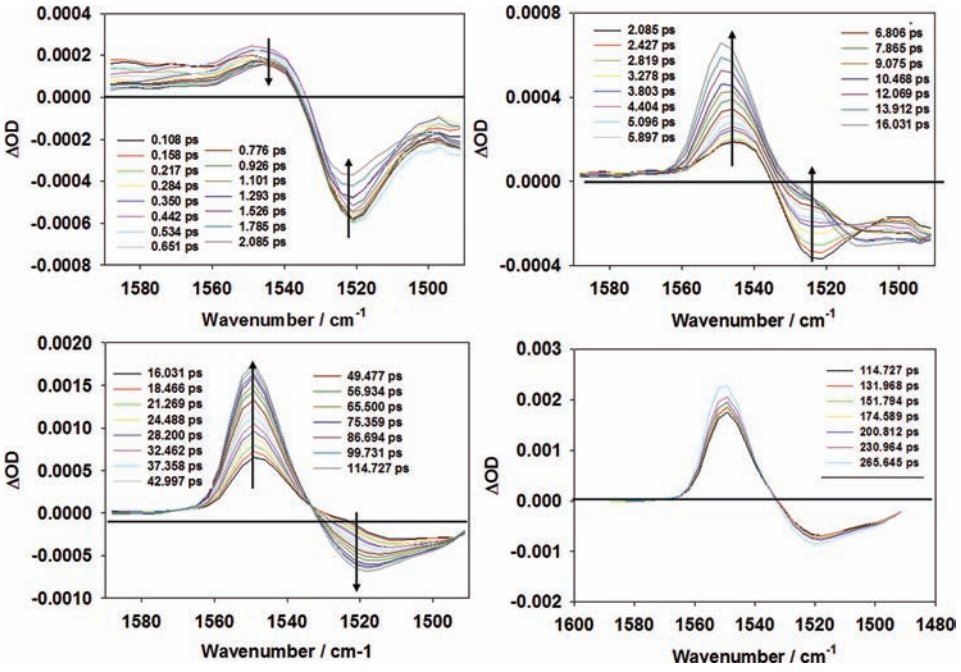

Figure 3. TRIR spectra of **I** collected in THF at room temperature at various delay times: initial spectra (top, left); growth of $^1(\delta \rightarrow \delta^*)$ and $^3(\delta \rightarrow \delta^*)$ states (top, right); interconversion between $^1(\delta \rightarrow \delta^*)$ and $^3(\delta \rightarrow \delta^*)$ states (bottom, left); long-lived spectrum (bottom, right).

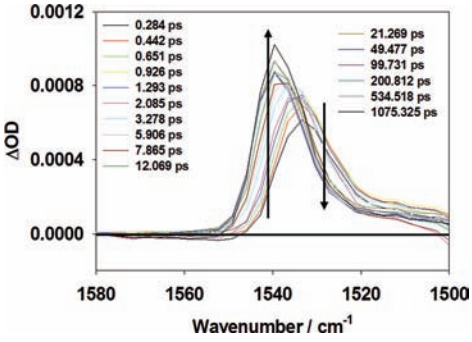

Figure 4. TRIR spectra of **II** in THF at room temperature.

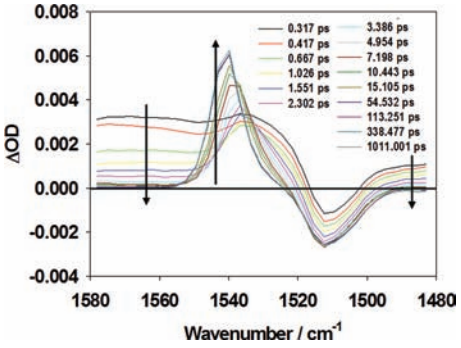

Figure 5. TRIR spectra for **III** in THF at room temperature.

tungsten. One indication has been the lifetimes of the T_1 state, obtained by nanosecond transient absorption (ns-TA) spectroscopy, where long ~50−100 μs lifetimes indicate $^3(\delta \rightarrow \delta^*)$ states and shorter 10−300 ns lifetimes indicate ^{3}MLCT states. This was also seen for compounds **III** and **IV**, and values for $\tau(T_1)$ = 58 and 0.058 μs, respectively, were found supporting the assignment above.[17] These types of measurements were

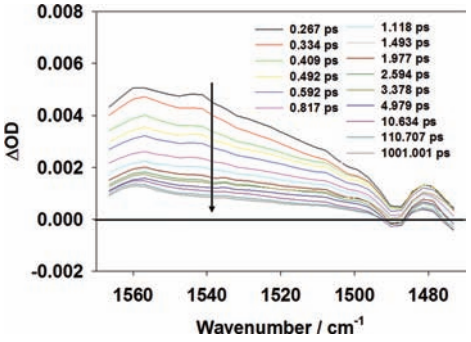

Figure 6. TRIR spectra of **IV** in THF at room temperature.

unsuccessful for **I** and **II**, on the other hand, making the use of TRIR even more important for these compounds.

Further support for the assignment of the state responsible for the peak occurring at 1540 cm^{-1} is found in a series of trans-bis-bis compounds with the formula *trans*-$Mo_2(L_1)_2(L_2)_2$, where L_1 and L_2 = 2,4,6-triisopropylbenzoate and *p*-cyanobenzoate, respectively, or acetate and $[(N^iPr)_2CC{\equiv}CC_6H_5]^-$, respectively. These two compounds have been well characterized by both electronic[19] and TRIR spectroscopy[20] and are believed to have T_1 as the $^3(\delta \rightarrow \delta^*)$ state. Their TRIR spectra between 1500 and 1600 cm^{-1} at long delay times are shown in Figure S1 in the Supporting Information, and each compound also possesses a peak near 1540 cm^{-1}.

The presence of the $^1(\delta \rightarrow \delta^*)$ state at relatively low energy in compounds **I**−**IV** provides additional possible decay pathways upon excitation into the ^{1}MLCT band. This makes the initial dynamics more interesting and complicated, so these have been presented for each compound separately and in more detail below.

fs-TRIR Spectroscopy: Initial Dynamics. *$Mo_2(O_2C^tBu)_4$ (I).* Figure 3 shows the TRIR spectra for **I**, and the corresponding kinetic traces are shown in Figure S2 in the Supporting Information. The dynamics for this compound are

dx.doi.org/10.1021/ic201957a | *Inorg. Chem.* 2012, 51, 491−498

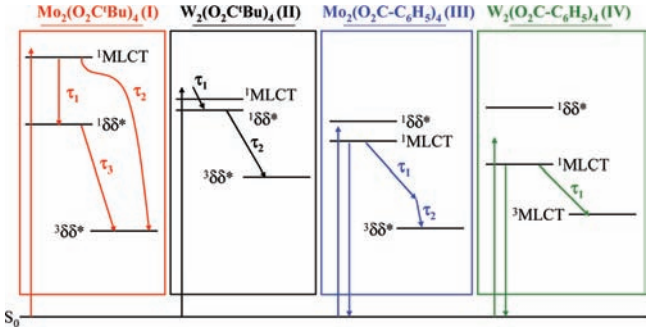

Figure 7. Jablonski diagrams for processes detected by TRIR spectroscopy.

particularly complicated, and so the spectra have been split up according to delay times that best represent the various processes. Spectra occurring between 0 and 2 ps are shown in the top left panel and show an initial bleaching at 1520 cm^{-1}, corresponding to $\nu_{as}(CO_2)$ in the ground state and an initial, broad absorption at higher wavenumber between 1540 and 1590 cm^{-1}. During the first 2 ps, the initial absorption slightly decays with a ~0.53 ps lifetime. The bleaching also recovers, but this process is not complete over the 2 ps window and continues as shown in the top right panel of Figure 3. This window shows delay times between 2 and 16 ps. An apparent band coincident with the bleaching grows in and is complete over this time period with a lifetime of ~5 ps. Also during this time, a resolved band at 1549 cm^{-1} grows in, but this process is not complete within this time window. The third time window is shown in the bottom left panel of Figure 3 and displays delay times between 16 and 115 ps. These spectra show now that the band coincident with the bleaching at ~1520 cm^{-1} begins to decay and, concomitantly, the band at 1549 cm^{-1} continues to grow in, resulting in an isosbestic point at 1535 cm^{-1}. Decay of the 1520 cm^{-1} band occurs with a 49.7 ps lifetime, whereas the band at 1549 cm^{-1} grows in with only a single lifetime of 40.9 ps, although the dynamics suggest that two processes lead to the formation of the 1549 cm^{-1} band. Indicated by the isosbestic point is the fact that the bands at 1549 and 1520 cm^{-1} originate from different excited states and the state responsible for the 1520 cm^{-1} band decays to populate the 1549 cm^{-1} band. However, because both bands grow in during the first 16 ps, this indicates that they are formed separately. The final set of delay points are shown in the bottom right panel of Figure 3 and show the long-lived band and ground-state bleaching associated with the $^3(\delta \rightarrow \delta^*)$ state as described above.

It is known that the S_1 state in **I** is the $^1(\delta \rightarrow \delta^*)$ state, and so an additional decay pathway is possible upon excitation into the ^{1}MLCT, S_2, state compared to previously studied compounds where S_1 is MLCT.[9] With that, it is apparent that, after ^{1}MLCT excitation, there are three other states at lower energy that could potentially be involved in the subsequent dynamics: the ^{3}MLCT, $^1(\delta \rightarrow \delta^*)$, and $^3(\delta \rightarrow \delta^*)$ states. Therefore, it is proposed that the observed dynamics fit the following pathway. Initial excitation produces a state characterized by the spectra during 0–2 ps. The initially formed excited-state population is "hot" and gives rise to broad features at early times that narrow as the molecule cools. Subsequently, the initial excited-state population bifurcates into two states, whose formations are observed from 2 to 16 ps. One state is assigned the lower-energy S_1, $^1(\delta \rightarrow \delta^*)$, state and forms with a 5 ps lifetime. The other state is assigned the lowest-energy T_1, $^3(\delta \rightarrow \delta^*)$, state and forms from the initial state with a 40 ps lifetime. Subsequently, the intermediate $^1(\delta \rightarrow \delta^*)$ state decays to form the $^3(\delta \rightarrow \delta^*)$ state with a 50 ps lifetime. This described pathway is represented in the left panel of Figure 7 (vide infra). Assuming this pathway is correct, the singlet (~1520 cm^{-1}) and triplet (~1549 cm^{-1}) $\delta\delta^*$ states have different $\nu_{as}(CO_2)$ wavenumbers. This result is not intuitively obvious from the simple molecular orbital picture shown in Figure 1. In the manifold of four states derived from the two-electron δ bond, the $^1(\delta \rightarrow \delta^*)$ state has primarily ionic MM character, whereas the $^3(\delta \rightarrow \delta^*)$ state has covalent character.[4] It is proposed that this difference in bonding character affects how well the MM δ orbitals can mix with the CO_2 π system and therefore affects the $\nu_{as}(CO_2)$ wavenumber.

Another possibility for the intermediate state at 1520 cm^{-1} is the ^{3}MLCT state. The appearance of $\nu_{as}(CO_2)$ at this frequency is unlikely assuming electronic delocalization across all four pivalate ligands in this state. In this situation, this vibration would be expected at lower wavenumber compared to the ground-state bleaching. It could also be possible, however, that the pivalate ligands in this ^{3}MLCT state are not extensively coupled together. In this case, unreduced or only slightly reduced pivalate ligands would have $\nu_{as}(CO_2)$ at slightly higher or similar wavenumber as the ground state. However, in $Ru(bpy)_3^{2+}$ complexes, this localization only takes place in the longest-lived, lowest-energy ^{3}MLCT state, and no such example is known by the authors of localization occurring in an intermediate state.[21,22] Furthermore, if the ^{3}MLCT state were involved, the data would suggest a T_2-T_1 lifetime of ~50 ps. This would seem too long for this internal conversion process.

The lifetimes of the processes involved in the dynamics of **I** obtained from the kinetic traces shown in Figure S2 in the Supporting Information are also noteworthy when compared to the others. Data for each compound are summarized in Table 1.

Table 1. Summary of Observed Lifetimes from TRIR Spectroscopy

compound	τ_1/ps	τ_2/ps	τ_3/ps
I	4.9 ± 0.2	40.4 ± 0.3	50 ± 2
II	<300 fs	4.3 ± 0.3	
III	2.5 ± 0.3	12.9 ± 0.3[a]	
IV	0.4 ± 0.1		

[a]Associated with vibrational cooling.

Normally, intersystem crossing (ISC) between the ^{1}MLCT state and the $^3(\delta \rightarrow \delta^*)$ state in these types of quadruply bonded compounds occurs in ~1–20 ps.[15,16,18] In this case for **I**, it appears to occur on a longer time scale of ~40 ps. This is attributed to the much larger energy difference between these two states in this compound. The onset of the $^1(\delta \rightarrow \delta^*)$ absorption occurs at ~460 nm and the onset of the $^3(\delta \rightarrow \delta^*)$ emission can be estimated by comparison to a similar compound, $Mo_2(T^iPB_4)$, as ~1120 nm. This gives an estimation of ~18 700 cm^{-1} for $\Delta E_{S_2-T_1}[^1\text{MLCT}-^3(\delta \rightarrow \delta^*)]$. The energy difference between the $^1(\delta \rightarrow \delta^*)$ and $^3(\delta \rightarrow \delta^*)$ states, $\Delta E_{S_1-T_1}[^1(\delta \rightarrow \delta^*)-^3(\delta \rightarrow \delta^*)]$, can be similarly estimated as 11 900 cm^{-1}. Although the energy difference is much smaller, the ISC process occurs with longer lifetime, 50 ps. This can be rationalized with El Sayed's rules, which state that intramolecular processes involving a change in the orbital

dx.doi.org/10.1021/ic201957a | Inorg. Chem. 2012, 51, 491–498

type (i.e., $\pi\pi^*-n\pi^*$) are enhanced and those that conserve the orbital type are slow.[23] Therefore, the S_2-T_1 conversion, which converts between M δ–L π^* (MLCT) and M δ–M δ^*, is the faster process. Compared to the ISC processes, the S_2-S_1 internal conversion occurs on a faster time scale of only 5 ps.

In the spectra of compounds **II**–**IV**, we can use the differences that appear in the IR spectral features to rationalize the assignments based on whether an MLCT or $\delta\delta^*$ state is occupied.

$W_2(O_2C^tBu)_4$ (II). With a change of the metal system to tungsten, the ^{1}MLCT absorption shifts to lower energy, while the $^1(\delta \rightarrow \delta^*)$ absorption shifts to higher energy. This can be inferred from the absorption spectra of the series $M_2(O_2C^tBu)_4$[9] and the $^3(\delta \rightarrow \delta^*)$ emission spectra of the series $M_2(T^iPB)_4$, where M_2 = Mo_2, MoW, or W_2.[14] For tungsten carboxylate compounds, the $^1(\delta \rightarrow \delta^*)$ state has not been directly observed by absorption, but the trend is also suggested by quantum chemical calculations. This means, even though the MLCT absorption occurs at higher energy compared to **III**, for this compound it is possible the ^{1}MLCT and $^1(\delta \rightarrow \delta^*)$ absorptions occur close in energy. Excitation at 400 nm, which is into the low-energy side of the ^{1}MLCT absorption, yields the TRIR spectra shown in Figure 4. The initial spectra consist solely of a resolved band at 1534 cm^{-1}. The bleaching occurs outside of the detection range at 1480 cm^{-1}, as observed in the ground-state IR spectrum. At increased delay times, the initial spectrum decays and a new band emerges while shifting to higher wavenumber. The final spectrum has a peak at 1540 cm^{-1}. Kinetic traces are shown in Figure S3 in the Supporting Information and show the lifetimes of the decay and rise of the initial and final spectra, respectively, with lifetimes of 3.4 and 5.3 ps.

The initial spectra for **II** can be contrasted with the spectra for compounds **III** and **IV** (below). In **III** and **IV**, the spectra are broad and featureless, whereas in **II**, the spectrum contains a sharp peak and, as explained below, these compounds (**III** and **IV**) are expected to have initial ^{1}MLCT states. This would imply that, even though excitation is into the ^{1}MLCT state, the initial spectrum observed, with a peak value of 1534 cm^{-1}, is actually due to the population of the $^1(\delta \rightarrow \delta^*)$ state and internal conversion occurs on an ultrafast time scale. It is thought that the shape and position of the spectrum imply this conclusion. Subsequently, the T_1 $^3(\delta \rightarrow \delta^*)$ state is formed with a vibrational absorption value at 1540 cm^{-1}. Similar to the molybdenum analogue, the singlet and triplet $\delta\delta^*$ states are shifted by different amounts compared to the ground-state value, with $^1(\delta \rightarrow \delta^*)$ shifted less. The lifetime of the ISC process between the $^1(\delta \rightarrow \delta^*)$ and $^3(\delta \rightarrow \delta^*)$ states can also be rationalized with that observed for **I**. Because of the presence of the heavier element, tungsten, the spin–orbit coupling between the $^1(\delta \rightarrow \delta^*)$ and $^3(\delta \rightarrow \delta^*)$ states is greater and the observed ISC process occurs with a shorter lifetime. The assigned pathway is represented in the middle left panel of Figure 7.

Alternatively, the observations described by Figure 4 could be described as a dynamic shift of the initial band at 1534 cm^{-1} to the long-lived band at 1540 cm^{-1}, which is consistent with vibrational cooling (VC) within one of the possible electronic states.[26] If this is the case, the dynamics simply consist of ultrafast ISC of less than ~150 fs to populate a hot triplet state with $\nu_{as}(CO_2)$ absorption at 1534 cm^{-1} and cooling over ~4 ps to give the relaxed T_1 $^3(\delta \rightarrow \delta^*)$ state at 1540 cm^{-1} and the WW $^1(\delta \rightarrow \delta^*)$ state is not observed. One way to distinguish the VC assignment would be to conduct the excitation wavelength dependence of the TRIR spectra. If VC does indeed cause the observed spectral changes, exciting with excess energy should result in an increase in the observed lifetime and magnitude of the shift in $\nu_{as}(CO_2)$. Therefore, further studies of **II** may be warranted.

$Mo_2(O_2C-C_6H_5)_4$ (III). With changes in the carboxylate ligand system, the $^1(\delta \rightarrow \delta^*)$ absorption usually has a very small change in energy but shifts slightly higher with the electron-withdrawing ability of the ligands.[24,25] In **III**, the ^{1}MLCT absorption is shifted to a similar region where the $^1(\delta \rightarrow \delta^*)$ absorption is expected and so the two states may lie close in energy. Excitation at 400 nm, on the high energy side of the ^{1}MLCT band, leads to the TRIR spectra in Figure 5. The initial spectra are broad and featureless, and the excited-state absorption extends across the entire detection range. There is also a feature corresponding to the ground-state bleaching of the $\nu_{as}(CO_2)$ vibration at 1512 cm^{-1}. The initial spectra decay according to the kinetic traces shown in Figure S4 in the Supporting Information with dual exponential lifetimes of ~0.35 and ~2.5 ps, measured at 1548 or 1488 cm^{-1}, for example. Subsequently, a sharp IR absorption feature grows in with a slight dynamic shift to a higher wavenumber settling at 1540 cm^{-1}. Kinetics measured at 1540 cm^{-1} show that this band grows in with a 12.9 ps lifetime and an ultrafast decay of 0.36 ps, similar to that observed at other wavenumbers.

The long-lived band is indicative of the T_1 state characterized as the $^3(\delta \rightarrow \delta^*)$ according to the discussion above. The shape of the spectrum in the short compared to the long time domains leads to the suggestion that the initial state is ^{1}MLCT. From the spectra of **I** and the long-lived spectra discussed above, the nature of the $\delta\delta^*$ states is a narrow spectrum with a resolved peak, and this is clearly not the case for the initial spectra of **III**. Furthermore, compared to **I**, the initial broad spectra are more intense and better represented. This could be due to the presence of additional vibrations in the benzoate ligands that occur in this region of the spectrum. Namely, the symmetric and asymmetric ν(C=C) of the phenyl rings, which generally occur at ~1570 and 1600 cm^{-1}, respectively, would be expected at lower frequency in the MLCT excited states. This could be responsible for the broadness of the spectra. Although these phenyl ring vibrations are very weak in the ground-state IR spectrum, their intensities could be significantly enhanced by the new electronic environment of the ^{1}MLCT state with a larger dipole moment. Their bandwidths could also become significantly larger, which is typical of excited states that represent a significant change in the electronic distribution, and this feature could contribute to the broad, featureless spectra that are observed in the MLCT states.[26]

Another possibility for the broad spectra that appear in the ^{1}MLCT state from 1580 to 1480 cm^{-1} is an electronic rather than a vibrational transition. From Figure 1, it can be seen that there are other unoccupied orbitals lying close in energy to the L π^* e_u orbital, such as the L π^* a_{2g} and b_{2g} orbitals. Promotion of an electron from the e_u orbital in the MLCT state to either of these orbitals represents an allowed transition with *xy* polarization in the D_{4h} point group. On the basis of the calculated orbital energies, the transition to the lower-energy a_{2g} orbital would occur at ~3400 cm^{-1} in the IR region. While this value for the energy does not agree with the observed frequency range, it does support the possibility that such electronic transitions could be observed in the TRIR experi-

dx.doi.org/10.1021/ic201957a | *Inorg. Chem.* 2012, 51, 491–498

ment. Further experimental or more detailed computational work is needed to confirm this possibility.

The observed dynamics described above suggest the photophysical pathway represented in the middle right panel of Figure 7 (vide infra). Initial excitation produces the ^{1}MLCT state. This state undergoes ISC with an observed lifetime of ~2.5 ps to the $^3(\delta \rightarrow \delta^*)$ state, which eventually gives the peak at 1540 cm^{-1}. The shorter lifetime compared to the equivalent process for **I** is possibly due to the smaller energy gap between the ^{1}MLCT and $^3(\delta \rightarrow \delta^*)$ states and the nature of the conversion involving a change in the orbital type. The growth of the 1540 cm^{-1} peak, however, clearly occurs with a dynamic shift, and measuring the kinetics at this wavelength gives a 12.5 ps rise component. The dynamic shift to higher frequency is consistent with VC within the $^3(\delta \rightarrow \delta^*)$ state and so ISC must occur to a nonequilibrated hot state that then further relaxes.[27] Furthermore, the fact that excitation at 400 nm occurs on the high-energy side of the ^{1}MLCT band gives an additional incentive for the ISC process to occur directly to a vibrationally excited level in the $^3(\delta \rightarrow \delta^*)$ state and increases the likelihood that VC is observed in this compound.

$W_2(O_2C-C_6H_5)_4$ (IV). In **IV**, the metal has two effects on the lowest-energy absorptions. First, the $^1(\delta \rightarrow \delta^*)$ transition goes to higher energy and, second, the ^{1}MLCT transition goes to lower energy compared to the molybdenum analogue. The lower energy of the benzoate π^* orbitals further increases separation of the $^1(\delta \rightarrow \delta^*)$ and ^{1}MLCT states compared to **III**. Excitation at 514 nm, therefore, excites the ^{1}MLCT transition, and the $^1(\delta \rightarrow \delta^*)$ state is expected at higher energy. The TRIR spectra following this excitation are shown in Figure 6 and corresponding kinetic traces in Figure S5 in the Supporting Information. The initial spectrum consists now of a very broad, featureless, spectrum with a small cut-out corresponding to the ground-state $\nu_{as}(CO_2)$ bleaching at 1490 cm^{-1}. Kinetic traces show only a single ultrafast decay of 0.39 ps to leave a final, long-lived spectrum that is similar in both shape and breadth. This spectrum leads to the conclusion that the lowest-energy T_1 state has become ^{3}MLCT. The combination of using both the tungsten metal center and the benzoate ligands with lower-energy π^* orbitals has caused the reversal of states in **IV** compared to **II**. The lifetime of the ^{1}MLCT state has also become smaller in **IV** compared to **II**. This can be attributed to the increased spin−orbit coupling between these two states when using the tungsten metal center.

Similar to the statements made for **III**, the nature of the observed TRIR signal can be associated with an electronic transition occurring between the L π^* e_u orbital in the MLCT state and another closely lying unoccupied orbital. From Figure 1, it can be seen that changing the metal from Mo to W results in the M π^* e_g orbital going to higher energy, occurring now above the L π^* e_u orbitals. A transition occurring from the L π^* e_u orbital to the M π^* e_g orbital is also allowed but with z polarization. The MLCT excited tungsten compound additionally has available the allowed transitions mentioned above for **III**, those that occur to the L π^* a_{2g} and b_{2g} orbitals. On the basis of calculated orbital energies, the lowest-energy excited-state transition is to the M π^* e_g orbital and is estimated to occur at 722 cm^{-1}. The transition to the L π^* a_{2g} orbital is estimated to occur at energy similar to that of the molybdenum analogue, **III**, ~3400 cm^{-1}. This excited-state transition to the L π^* a_{2g} orbital could be a likely possibility given that the observed signal is in a similar part of the spectrum for both **III** and **IV**. For **IV**, the S_1 and T_1 states are both MLCT in nature, and so each state is represented by the broad and featureless electronic absorption.

CONCLUSIONS

The Jablonski diagram shown in Figure 7 represents the changes incurred to the relative excited-state energies upon variation of the metal center and ligand system and follows the expectations set out by the molecular orbital diagram of Figure 1. As the energy of the ligand π^* orbital is lowered by increasing the extent of π conjugation, as with using benzoate relative to pivalate ligands, the energy of the MLCT state decreases. Alternatively, changing the metal to tungsten increases the energy of the δ-based HOMO, causing additional relative stabilization of the MLCT state. Furthermore, with tungsten, the δ^* orbital is also increased in energy, to a larger extent than the δ-based HOMO, and the $\delta\delta^*$ state increases in energy.[14] As a consequence of these properties, the observed photophysical pathways can be varied.

The spectra of **I** were particularly interesting in that, if the proposed pathway is correct, two different ISC processes were observed within the same molecule. This could, perhaps, allow for generalizations to be made concerning the lifetimes of fundamental photophysical processes between the electronic excited states of different types in association with El Sayed's rules.[28] Also, in both **I** and **II**, both the singlet and triplet $\delta\delta^*$ states were observed, whose detection has been the topic of research since the initial discovery of the quadruple bond some 40 years ago.[29−31] In **III** and **IV**, the benzoate ligands bring down the ^{1}MLCT energy such that it is the S_1 state, eliminating the pathway through the $^1(\delta \rightarrow \delta^*)$ state. However, within the triplet manifold, this stabilization is not sufficient for the MLCT state to become T_1 for **III**, and instead it is $^3(\delta \rightarrow \delta^*)$. In **IV**, the energy reduction of the MLCT states is larger and T_1 finally becomes MLCT.

The motivation for using TRIR spectroscopy in our group has been, in general, to study the electronic delocalization and more specifically the electronic coupling between identical and interchangeable redox-active groups within individual molecules involving quadruple bonds. We have done this previously for *trans*-bis-bis compounds where the coupling and delocalization of an excited electron across the two trans ligands through the metal−metal quadruply bonded system was evaluated.[20] We also hope to study compounds of the type $[M_2(O_2CR)_3]_2(\mu\text{-}O_2CBCO_2)$, where M = Mo or W, R = ^{t}Bu, and B = conjugated organic, commonly known as "dimers-of-dimers", whose mixed-valence, singly oxidized states have already been studied in some detail.[32,33] In these systems, excitation also leaves a positive charge on either one metal center or both in the MLCT or metal-centered $\delta\delta^*$ states, providing a mixed-valence system. The observation of $\nu_{as}(CO_2)$ in the excited states of the molecules in this study has allowed TRIR signals observed in the neighborhood of 1540 cm^{-1} to be identified as a general signature of the $\delta\delta^*$ states. These signals should also greatly aid in the interpretation of the TRIR results of dimer-of-dimers, which employ similar carboxylate spectator ligands, and these studies are planned for the near future.

ASSOCIATED CONTENT

Supporting Information

TRIR spectra for *trans*-$Mo_2(L_1)_2(L_2)_2$ and kinetic traces for I−IV. This material is available free of charge via the Internet at http://pubs.acs.org.

dx.doi.org/10.1021/ic201957a | *Inorg. Chem.* 2012, 51, 491−498

AUTHOR INFORMATION

Corresponding Author

*E-mail: chisholm@chemistry.ohio-state.edu (M.H.C.), gustafson@chemistry.ohio-state.edu (T.L.G.).

ACKNOWLEDGMENTS

This paper is dedicated to Carlos A. Murillo on the occasion of his 60th birthday. This material is based upon work supported by the National Science Foundation under Grant CHE-0957191. The work was performed at The Ohio State University, partly in the Center for Chemical and Biophysical Dynamics. We thank The Ohio State University Institute for Materials Research and the Wright Center for Photovoltaic Innovation and Commercialization for financial support and the Ohio Supercomputing Center for computational resources.

REFERENCES

(1) Hopkins, M. D.; Gray, H. B.; Miskowski, V. M. *Polyhedron* **1987**, *6*, 705−714.
(2) Engebretson, D. S.; Zaleski, J. M.; Leroi, G. E.; Nocera, D. G. *Science* **1994**, *265*, 759−762.
(3) Cotton, F. A.; Nocera, D. G. *Acc. Chem. Res.* **2000**, *33*, 483−490.
(4) Cotton, F. A.; Murillo, C. A.; Walton, R. A. *Multiple Bonds Between Metal Atoms*, 3rd ed.; Springer Science and Business Media, Inc.: New York, 2005.
(5) Clark, R. J. H.; Hempleman, A. J.; Kurmoo, M. *J. Chem. Soc., Dalton Trans.* **1988**, 973.
(6) Kukura, P.; McCamant, D. W.; Mathies, R. A. *Annu. Rev. Phys. Chem.* **2007**, *58*, 461−488.
(7) McCamant, D. W.; Kukura, P.; Yoon, S.; Mathies, R. A. *Rev. Sci. Instrum.* **2004**, *75*, 4971−4980.
(8) McCarley, R. E.; Templeton, J. L.; Colburn, T. J.; Katovic, V.; Hoxmeier, R. J. *Adv. Chem. Ser.* **1976**, *150*, 318−334.
(9) Santure, D. J.; Huffman, J. C.; Sattelberger, A. P. *Inorg. Chem.* **1985**, *24*, 371−378.
(10) Cotton, F. A.; Wang, W. *Inorg. Chem.* **1984**, *23*, 1604−1610.
(11) Frisch, M. J.; et al. Gaussian, Inc.: Wallingford, CT, 2004.
(12) Burdzinski, G.; Hackett, J. C.; Wang, J.; Gustafson, T. L.; Hadad, C. M.; Platz, M. S. *J. Am. Chem. Soc.* **2006**, *128*, 13402−13411.
(13) Wang, J.; Burdzinski, G.; Kubicki, J.; Platz, M. S. *J. Am. Chem. Soc.* **2008**, *130*, 11195−11209.
(14) Alberding, B. G.; Chisholm, M. H.; Chou, Y.-H.; Gallucci, J. C.; Ghosh, Y.; Gustafson, T. L.; Patmore, N. J.; Reed, C. R.; Turro, C. *Inorg. Chem.* **2009**, *48*, 4394−4399.
(15) Alberding, B. G.; Chisholm, M. H.; Ghosh, Y.; Gustafson, T. L.; Liu, Y.; Turro, C. *Inorg. Chem.* **2009**, *48*, 8536−8543.
(16) Alberding, B. G.; Barybin, M. V.; Chisholm, M. H.; Gustafson, T. L.; Reed, C. R.; Robinson, R. E.; Patmore, N. J.; Singh, N.; Turro, C. *Dalton Trans.* **2010**, *39*, 1979−1984.
(17) Byrnes, M. J.; Chisholm, M. H.; Gallucci, J. A.; Liu, Y.; Ramnauth, R.; Turro, C. *J. Am. Chem. Soc.* **2005**, *127*, 17343−17352.
(18) Alberding, B. G.; Chisholm, M. H.; Chou, Y.-H.; Ghosh, Y.; Gustafson, T. L.; Liu, Y.; Turro, C. *Inorg. Chem.* **2009**, *48*, 11187−11195.
(19) Alberding, B. G.; Chisholm, M. H.; Gustafson, T. L.; Liu, Y.; Reed, C. R.; Turro, C. *J. Phys. Chem. A* **2010**, *114*, 12675−12681.
(20) Alberding, B. G.; Chisholm, M. H.; Gallucci, J. C.; Ghosh, Y.; Gustafson, T. L. *Proc. Natl. Acad. Sci. U.S.A.* **2011**, *108*, 8152−8156.
(21) Wallin, S.; Davidsson, J.; Modin, J.; Hammarström, M, L. *J. Phys. Chem. A* **2005**, *109*, 4697−4704.
(22) Yeh, A. T.; Shank, C. V.; McCusker, J. K. *Science* **2000**, *289*, 935−938.
(23) El-Sayed, M. A. *J. Chem. Phys.* **1963**, *38*, 2834−2838.
(24) Martin, D. S.; Newman, R. A.; Fanwick, P. E. *Inorg. Chem.* **1979**, *18*, 2511−2520.
(25) Trogler, W. C.; Solomon, E. I.; Trajberg, I.; Ballhausen, C. J.; Gray, H. B. *Inorg. Chem.* **1977**, *16*, 828−836.
(26) Turner, J. J. *Coord. Chem. Rev.* **2002**, *230*, 213−224.
(27) Hamm, P.; Ohline, S. M.; Zinth, W. *J. Chem. Phys.* **1997**, *106*, 519−529.
(28) El-Sayed, M. A. *J. Chem. Phys.* **1962**, *36*, 573.
(29) Cotton, F. A.; Curtis, N. F.; Harris, C. B.; Johnson, B. F. G.; Lippard, S. J.; Mague, J. T.; Robinson, W. R.; Wood, J. S. *Science* **1964**, *145*, 1305−1307.
(30) Miskowski, V. M.; Goldbeck, R. A.; Kliger, D. S.; Gray, H. B. *Inorg. Chem.* **1979**, *18*, 86−89.
(31) Bradley, P. M.; Smith, L. T.; Eglin, J. L.; Turro, C. *Inorg. Chem.* **2003**, *42*, 7360−7362.
(32) Chisholm, M. H.; Patmore, N. J. *Acc. Chem. Res.* **2007**, *40*, 19−27.
(33) Lear, B. J.; Chisholm, M. H. *Inorg. Chem.* **2009**, *48*, 10954−10971.